JOURNAL OF APPLIED ELECTROCHEMISTRY **27** (1997) 939–946

Current efficiency in the Hall–Héroult process for aluminium electrolysis: experimental and modelling studies

P. A. SOLLI

Hydro Aluminium, PO Box 303, N-5870 Øvre Årdal, Norway

T. EGGEN, E. SKYBAKMOEN

SINTEF Materials Technology, Electrolysis Group, N-7034 Trondheim, Norway

Å. STERTEN

Department of Electrochemistry, The Norwegian Institute of Technology, N-7034 Trondheim, Norway

Received 1 July 1996; revised 21 November 1996

Results are presented from a laboratory study of the influence of electrolyte composition, temperature, cathodic current density and interpolar distance on the current efficiency with respect to aluminium (CE). The current efficiency was determined from the weight gain of metal, in a laboratory cell designed to attain good and reproducible convective conditions, and with a flat cathode surface which ensures uniform cathodic current distribution. The cell is believed to more closely represent conditions in industrial cells than traditional small-scale cells, and is a good basis for an experimental study of the influence of isolated variable parameters on the current efficiency with respect to aluminium. The results show a nonlinear decrease of CE with increasing electrolyte temperature, a close to linear decrease of CE with increasing NaF/AlF_3 ratio in the electrolyte, a slight increase of CE with increasing electrolyte CaF_2 concentration, and no influence of electrolyte Al_2O_3 concentration on CE. A current efficiency model, based on previous work and theory of electrochemistry and mass transport, shows good agreement with the obtained results.

List of symbols

a_i	activity of component i in bulk of electrolyte
c_i	concentration of component i in the electrolyte (wt %)
d	interpolar distance (cm)
F	Faraday constant (C mol^{-1})
i_{Al}	local current density for the aluminium deposition reaction (A cm^{-2})
i_{loss}	local current density for all cathodic side reactions (A cm^{-2})
i_{sc}	local current density due to short circuits and dispersion of metal (A cm^{-2})
i_c	local cathodic current density (A cm^{-2})
k_{mix}	local mixed mass transfer coefficient or rate constant (mol $cm^{-2}s^{-1}$)
r	molar ratio $n(NaF)/n(AlF_3)$
t	temperature (°C)
T	temperature (K)
x_{NaF}	molar fraction of NaF in the $NaF–AlF_3$ system
y	empirical sodium activity exponent

Greek letters

α	ratio between real sodium activity in bulk electrolyte and the corresponding activity when equilibrated with liquid Al of unit activity, $\alpha = (a_{Na,bulk})/(a_{Na,eq})$
ε	local current efficiency for the aluminium deposition reaction (%)
η	concentration overpotential/polarization (V)

1. Introduction

Industrial production of aluminium is exclusively based on the Hall–Héroult process. The process involves electrochemical decomposition of alumina (Al_2O_3) dissolved in cryolite (Na_3AlF_6) containing additives (AlF_3 and one or more of the following: CaF_2, MgF_2, LiF). The consumable carbon anode liberates CO_2 with a current efficiency close to 100% [1], while the cathodic current efficiency (CE) with respect to aluminium normally ranges from 87 to 96% in commercial cells. The main overall cell reaction may be written as

$$Al_2O_3 + 3/2C = 2Al + 3/2CO_2 \quad (1)$$

In previous papers [2, 3] probable mechanisms for the loss of current efficiency have been discussed based on previous work in the field. These papers

conclude that cathodic current normally is consumed by (i) the aluminium deposition reaction, and (ii) reduction reactions with formation of so-called dissolved metal species or reduced entities. The rate determining steps for the aluminium deposition process in commercial cells,

$$AlF_3 + 3Na^+ + 3e^- = Al + 3NaF \qquad (2)$$

are mainly mass transport of aluminium fluoride to the metal surface, and mass transport of sodium fluoride away from the metal surface. Modelling of the cathode process and loss of Faradaic efficiency [3] predicts that CE is a function of current density, cathode overvoltage, temperature, electrolyte composition and mass transfer coefficients.

Solli *et al.* [4] demonstrated the performance of a new and improved laboratory cell, specifically designed for determination of CE as a function of isolated variable parameters in the Hall–Héroult process. The anode was designed to give enhanced and reproducible bubble induced electrolyte convection, while the wettable cathode substrate gave a well defined cathode area, and thus a uniform current density. Low and consistent values of cathode polarization, as well as high and reproducible values of current efficiency were obtained with the laboratory cell.

The present paper is the fourth in a series concerning CE in the electrowinning of aluminium, and presents results of a laboratory study of CE as a function of temperature, bath composition, cathode polarization, cathodic current density and interpolar distance. Experimental values of current efficiency are compared with model calculations.

2. Experimental details

The laboratory cell is shown in Fig. 1. The graphite anode was designed to give enhanced and reproducible bubble induced convection, and was cylindrically shaped with a vertical hole through the centre. Two horizontal holes were machined perpendicular to each other, and perpendicular to the vertical hole, while the bottom of the anode was shaped with a slight inward slope towards the central vertical hole. The design was supposed to lead most of the anode gas bubbles up through the central hole, and to set up electrolyte flow as indicated by the arrows in Fig. 1.

The cathode was aluminium wetted on a stainless steel plate. This ensured a close to flat aluminium surface, and consequently an even current distribution on the cathode surface. The steel plate rested on a layer of alumina on top of a lining of high purity cast alumina cement. This arrangement ensured negligible transport of aluminium and electrolyte down to the graphite crucible, and a minimum of metal loss due to formation of aluminium carbide.

The cell was placed in a vertical tube furnace, and positioned to avoid temperature gradients in the electrolyte. The furnace was flushed with argon, and a small inert gas flow maintained through the furnace during electrolysis.

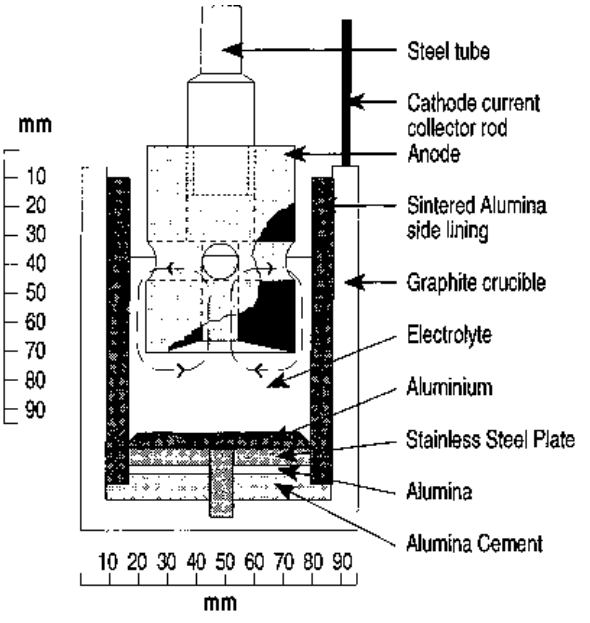

Fig. 1. Laboratory cell with electrolyte circulation pattern indicated by dotted lines and arrows.

The current was supplied by a d.c. power supply, and monitored as the voltage drop over a standardized resistance (Croydon Precision Instruments, 0.05 Ω, max. 50 A) in series with the cell circuit. The cathodic current density was referred to the inner cross-sectional area of the sintercorundum side lining. Alumina was regularly supplied through the central vertical hole of the anode. The duration of each electrolysis experiment was 4 h. Chemicals used were cryolite (Na_3AlF_6, natural hand-picked), AlF_3 (sublimated), Al_2O_3 (calcined) and CaF_2 of high purity.

After electrolysis the furnace with its contents were left to cool, after which the crucible was dissected and the solidified metal (Al and Fe) removed and cleaned of residual bath. The cleaned and dried metal was weighed, and CE calculated from the ratio of metal produced, to the theoretical amount given by Faraday's law of electrolysis.

The standard or basic electrolysis conditions were as follows: NaF/AlF_3 molar ratio (r) 2.5, Al_2O_3 concentration ($c_{Al_2O_3}$) 4 wt %, CaF_2 concentration (c_{CaF_2}) 5 wt %, temperature (t) 980 °C, cathode current density (i_c) 0.85 A cm^{-2} and interpolar distance (d) 2.7 cm. These variables were changed sequentially to study the isolated effect of each one of them on CE.

Employment of a sintercorundum (Al_2O_3) side lining leads partly to its dissolution, although slow, into the electrolyte. Analysis of the electrolyte at the end of experiments with presumed (weighed out) concentrations of 4 wt % alumina, revealed alumina concentrations in the order of 4–6 wt %, i.e. slightly higher than the weighed out amount.

Investigation of the influence of alumina concentration on CE was carried out in a pyrolytic boron nitride crucible (type PBN, SINTEC Keramik GmbH), where good control of the alumina concentration was possible.

3. Results and discussion

3.1. *CE model*

A description of the cathode processes including loss of current efficiency has been given in previous papers [2, 3]. Derivation of basic equations in the mathematical CE model was given in [3, 5]. Current efficiency was defined by the following relation:

$$\varepsilon = \frac{100 i_{Al}}{i_c} = \frac{100 i_{Al}}{i_{Al} + i_{loss} + i_{sc}} \quad (3)$$

where i_c is the local cathodic current density, i_{Al} is the local partial current density for the aluminium deposition reaction, i_{loss} is the local partial current density for all cathodic loss reactions and i_{sc} represents other losses due to local short circuits or dispersion of metal droplets in the electrolyte. For uniform cathode current density, and assuming no short circuits or metal dispersion, a simplified set of model equations will be used, where current efficiency is defined by

$$\varepsilon = \frac{i_c - i_{loss}}{i_c} \times 100 \quad (4)$$

The partial current density for cathodic loss reactions, i_{loss}, is described by Equation 5 [3, 5]:

$$i_{loss} = F\, k_{mix} a_{Na,eq}^{y} \left[-\alpha^{y} + \exp\left(\frac{-F\eta y}{RT}\right)\right] \quad (5)$$

where F is Faraday's constant, k_{mix} is a mixed mass transfer coefficient (or a mixed rate constant) defined by this equation, $a_{Na,bulk}$ is the activity of sodium in the bulk phase of the electrolyte, y is an empirical sodium activity exponent [3], η is the concentration overvoltage [6] referred to Reaction 2 and α is the fraction of sodium activity in the bulk phase ($a_{Na,bulk}$), to the corresponding equilibrium activity of sodium ($a_{Na,eq}$), referred to unit activity of aluminium,

$$\alpha = \frac{a_{Na,bulk}}{a_{Na,eq}} \quad (6)$$

The fraction α in Equation 6 is assumed to be zero, which means that the bulk of the electrolyte contains very small equilibrium concentrations of dissolved aluminium metal species [3, 5] during electrolysis. This gives for the partial current density of all cathodic loss reactions, i_{loss}:

$$i_{loss} = F\, k_{mix} a_{Na,eq}^{y} \exp\left(\frac{-F\eta y}{RT}\right) \quad (7)$$

The equilibrium activity of sodium (standard state pressure of 1 bar, unit activity aluminium) in the NaF–AlF_3–Al system, $a_{Na,eq}$ (binary) is described by Equation 8 [3],

$$a_{Na,eq}(\text{binary}) = \exp\left[50.633 + \frac{-50498 + 44000 x_{NaF}}{T} - \frac{9.9 + 35 x_{NaF}^2}{x_{NaF}}\right] \quad (8)$$

where T is the temperature in Kelvin and x_{NaF} related to the NaF/AlF_3 molar ratio (r) by

$$x_{NaF} = \frac{r}{r+1} \quad (9)$$

In the NaF–AlF_3–Al_2O_3–CaF_2–Al system the activity of sodium is not precisely known. However, from previous work [7, 8] the following empirical relationship was found for the influence of CaF_2 and Al_2O_3 on the equilibrium activity of sodium, $a_{Na,eq}$,

$$a_{Na,eq} = a_{Na,eq}\ (\text{binary}) \times \exp\left[-\frac{\text{wt \%}CaF_2}{19} + \frac{\text{wt \%}Al_2O_3}{85}\right] \quad (10)$$

The model parameters k_{mix} and y in Equation 7 were determined by a method of trial and error from results of the following data: (i) CE as a function of cathode current density, (ii) cathode polarization as a function of cathode current density, (iii) CE as a function of NaF/AlF_3 ratio, and (iv) CE as a function of temperature for three different NaF/AlF_3 ratios. All the above dependencies were sequentially determined in the laboratory cell under controlled electrolysis conditions.

The mixed mass transfer coefficient or rate constant k_{mix} was found to be temperature dependent:

$$k_{mix} = 0.432 \exp\left[-\frac{15000}{T}\right] \quad (11)$$

The exponent y in Equation 7 was found to be close to 0.5, but slightly dependent on NaF/AlF_3 ratio. The following equation gave a satisfactory fit to the results:

$$y = 0.38 + 0.045\, r \quad (12)$$

In agreement with previous work [9, 10], it was found that cathode polarization, η, was dependent on NaF/AlF_3 ratio, as shown in the section below. The following empirical equation was fitted to the measured polarization data:

$$\eta/\text{V} = 0.0015\, r - \frac{0.147 r i_c}{1.97 r - 1} \quad (13)$$

The Equations (4, 7–13) thus constitute the CE model used in the present work.

3.2. *Cathode polarization*

Cathode polarization was measured by a transient potential jump technique in the present laboratory cell, as described elsewhere [4]. Figure 2 shows experimental values and lines represented by Equation 13, for cathode polarization as a function of cathode current density. Each experimental value represents the average of 10–20 polarization readings, with standard deviation from the average varying between 10 and 20% (between 5 and 15 mV at industrial current densities) [4].

3.3. *Current efficiency as a function of cathodic current density*

Figure 3 shows experimental values and model predictions of CE as a function of cathodic current

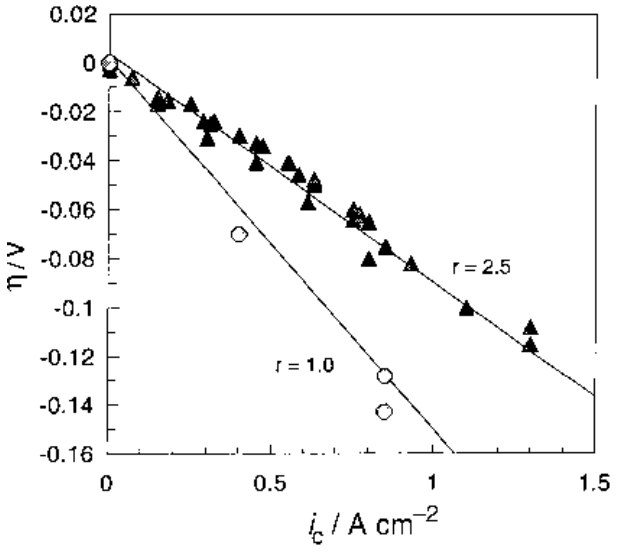

Fig. 2. Cathode polarization, η, as a function of cathodic current density, i_c, at NaF/AlF_3 molar ratio $r = 2.5$ and $r = 1.0$, and temperature 980 °C. Points: Experimental values, lines: Equation 13 (see text).

density. The model is basically in agreement with experimental values, although bubble induced convection and mass transfer conditions may be different at low current densities. The possible decrease in the mass transfer coefficient, k_{mix}, towards low current densities is discussed in Section 3.9.

Similar trends to the one shown in Fig. 3 have been obtained by other workers [11, 12].

3.4. *Electrolyte NaF/AlF$_3$ ratio*

Figure 4 shows CE as a function of NAF/AlF_3 molar ratio at constant 980 °C temperature; experimental values and model predictions. CE roughly follows a straight line, with slope $dCE/dr = -4.2\%$ per unit

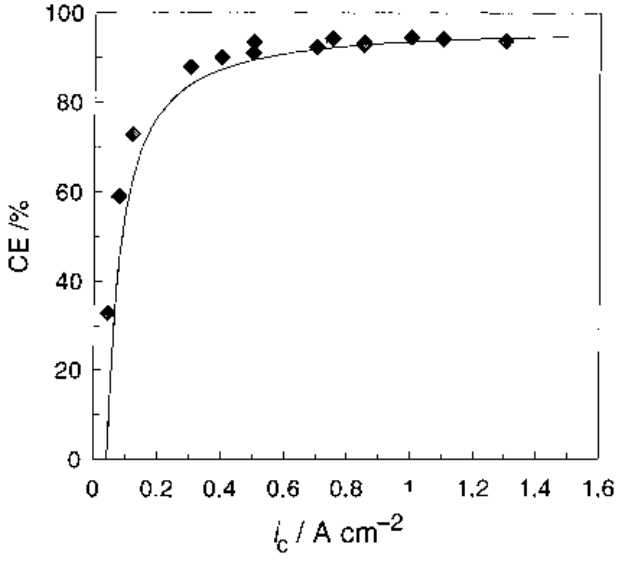

Fig. 3. Current efficiency, CE, as a function of cathodic current density, i_c. Temperature 980 °C, NaF/AlF_3 molar ratio 2.5, 5 wt% CaF_2 and 4 wt% Al_2O_3. Experimental values (points) and model curve (see text).

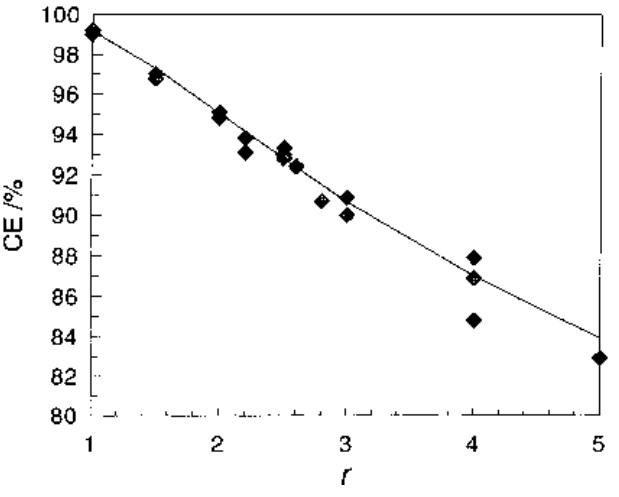

Fig. 4. Current efficiency, CE, as a function of NaF/AlF_3 molar ratio, r. Cathodic current density 0.85 A cm^{-2}, temperature 980 °C, 5 wt% CaF_2 and 4 wt% Al_2O_3. Experimental values (points) and model curve.

ratio. Most of the experimental work previously carried out on CE as a function of electrolyte NaF/AlF_3 ratio shows, in agreement with present work, a substantial increase of CE with increasing AlF_3 concentration in the electrolyte [13–17]. The effect of ratio (bath acidity) on CE reflects the rate change of cathodic side reactions, mainly due to significant increase of equilibrium sodium concentration on the cathode aluminium, with increasing NaF concentration in the electrolyte.

3.5. *Electrolyte temperature*

CE as a function of temperature was determined for NaF/AlF_3 molar ratios 2.0, 2.5 and 3.0, in order to attain satisfactory cross-determination of the influence of temperature and bath acidity on current efficiency. Figure 5 shows experimental values and model predictions. The slope dCE/dt becomes increasingly more negative with increasing electrolyte acidity and increasing temperature, as shown by the model curves in Fig. 6.

Experimental studies of CE as a function of temperature in industrial cells [15, 16, 18, 19] show some discrepancies, probably due to difficulties with isolation of the temperature parameter from other dynamic cell variables during industrial operation. Coefficients, dCE/dT, vary from −0.09 to −0.23 % K^{-1}.

The influence of temperature on CE is due to the effect of temperature on the equilibrium concentration of sodium, and thus the effect on the rate of cathodic side reactions (flux of dissolved metal) including electronic conduction.

3.6. *Electrolyte calcium fluoride concentration*

The calcium fluoride concentration was varied between 0 and 20 wt %. The results given in Fig. 7 show a slight increase of CE with increasing CaF_2 con-

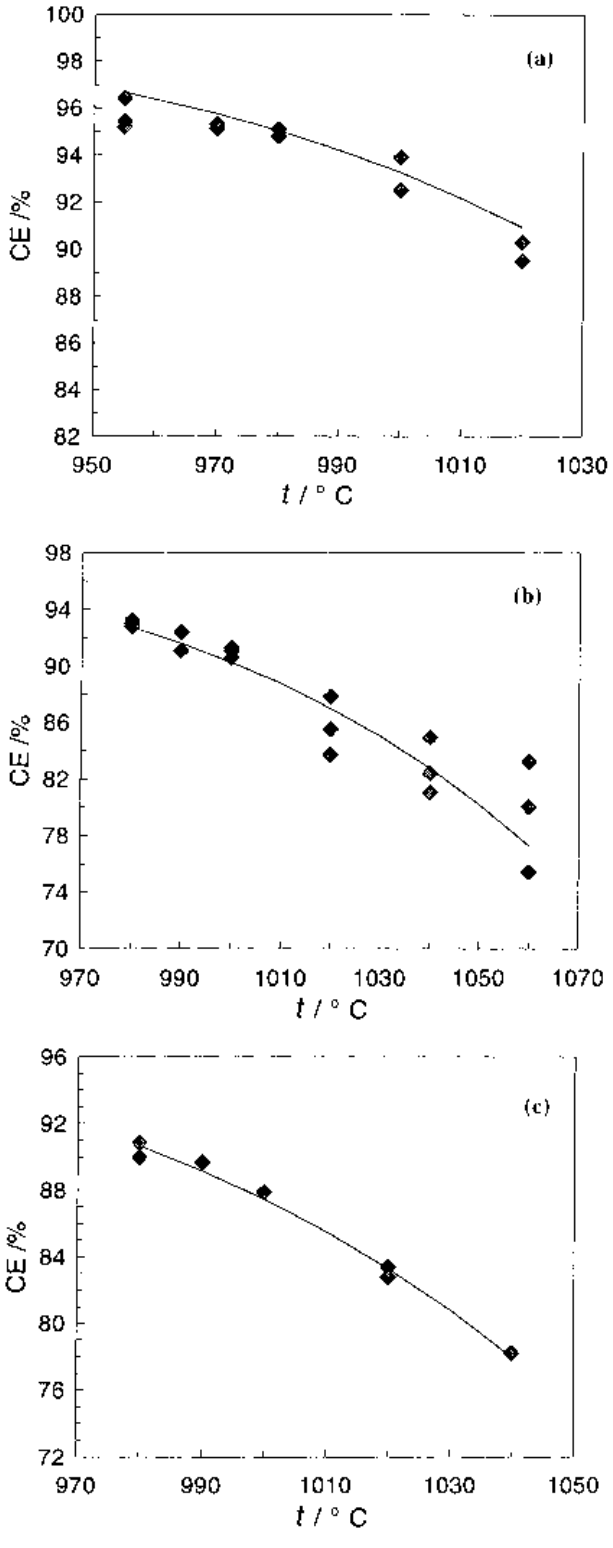

Fig. 5. Current efficiency, CE, as a function of temperature, t, at cathodic current density 0.85 A cm^{-2}, 5 wt% CaF_2 and 4 wt% Al_2O_3. (a) NaF/AlF_3 molar ratio, $r = 2.0$; (b) $r = 2.5$; and (c) $r = 3.0$. Experimental values (points) and CE model curves.

centration. The apparent discrepancy between model and experimental values at very low CaF_2 concentrations is discussed below (Section 3.9). There also appears to be a discrepancy between the model and experimental values at concentrations higher than 10 wt% CaF_2, and the single experimental values at 15 and 20 wt% are somewhat uncertain. There seems

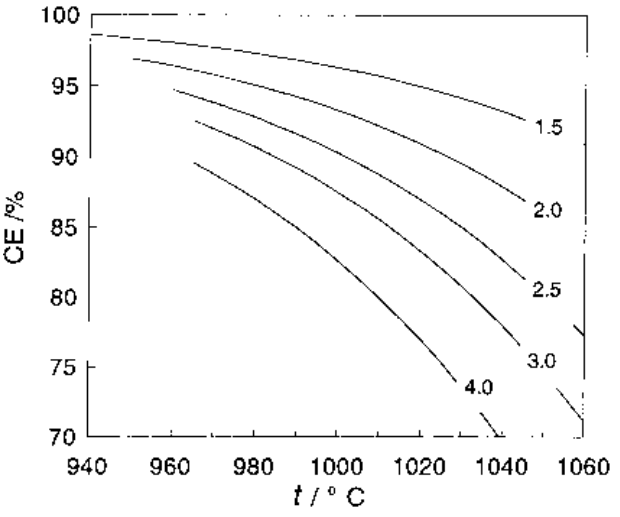

Fig. 6. Current efficiency, CE, as a function of temperature, t, at cathodic current density 0.85 A cm^{-2}, 5 wt% CaF_2 and 4 wt% Al_2O_3. CE model curves at NaF/AlF_3 molar ratio 1.5, 2.0, 2.5, 3.0 and 4.0.

to be a slight positive correlation between CE and CaF_2 concentration in the laboratory cell, although the slope is uncertain.

Previous results from CE studies in laboratory cells [20, 21] show increase in CE with increasing calcium fluoride concentration in the electrolyte, whereas studies in industrial cells [22, 23], over very limited ranges of concentration, show no measurable effect of CaF_2 on CE. Calcium fluoride concentrations higher than 7–10 wt% may in industrial cells cause excessive wave formation on the metal pad surface, with subsequent local events of short circuits or dispersion of metal droplets, and decrease of CE. This may occur due to increasing electrolyte density, giving a decrease in phase separation between the electrolyte and metal.

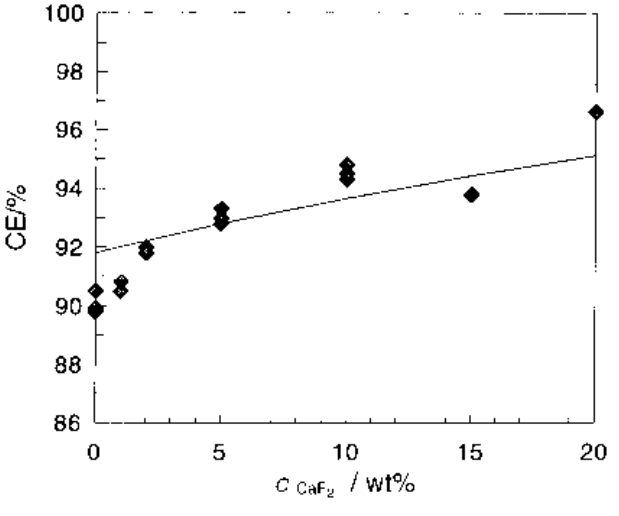

Fig. 7. Current efficiency, CE, as a function of electrolyte calcium fluoride concentration, c_{CaF_2}. Cathodic current density 0.85 A cm^{-2}, temperature 980 °C, 5 wt% CaF_2 and NaF/AlF_3 molar ratio 2.5. Experimental values (points) and model curve.

3.7. *Electrolyte alumina concentration*

The alumina concentration was varied between 1.2 and 8.0 wt% Al_2O_3. The results shown in Fig. 8 indicate that there is roughly no effect of alumina concentration on CE, within experimental uncertainties.

The constancy of the model line (slope close to zero) reflects that the equilibrium activity of sodium is only slightly affected by the alumina concentration. A least squares fit to the experimental data gave a slope $dCE/dc_{Al_2O_3}$ of ± 0.2% per wt%.

Results from previous investigations show considerable discrepancies as to the isothermal effect of alumina concentration on CE. Some results obtained in laboratory cells show a minimum in CE at 4–6 wt% alumina [20, 22], while others have found a positive correlation [11]. Most of the investigations in industrial cells show isothermal increase of current efficiency with increasing alumina concentration in the electrolyte [18, 19, 23, 24], with coefficients, $dCE/dc_{Al_2O_3}$, varying from 0.1 to 1.5% per wt% alumina. These measurements are based on analysis of the CO/CO_2 composition of the anode gases, and may be uncertain due to alumina concentration dependent changes in wetting properties between electrolyte and the anode carbon [25]. An increase in alumina concentration gives an increased wetting of carbon by the electrolyte and a decrease in the contact area between gas bubbles and carbon. This may cause a decrease in the transport rate of CO from the anode carbon pores into the anode gas bubbles, and thus a decrease of the CO content in the collected gases [25]. Leroy *et al.* [25] used a method of mass spectrometry and oxygen balance on collected anode gases, when they determined CE as a function of alumina concentration in industrial cells. They found a negative correlation between CE and alumina concentration, $dCE/dc_{Al_2O_3} = -2\%$ per wt% alumina. Due to the design of the present laboratory cell, it was not possible to try any of these gas analysis methods in the present study.

3.8. *Interpolar distance*

The interpolar distance was varied between 0.6 and 4.0 cm. The results given in Fig. 9 show that CE is constant for interpolar distances greater than 1.0 cm. At very low values (below 'critical interpolar distance'), where direct contact presumably is achieved between anode gas bubbles and the cathode boundary layer, a decrease of CE is observed. In commerical cells 'critical interpolar distances' may be in the order of 2 to 4 cm [19, 26], dependent on metal wave height or metal instability (i.e. magnetic busbar compensation, cell design, frozen side ledge geometry).

3.9. *Convection and interface mass transfer conditions*

In the present work current efficiency has been modelled assuming that the mass transfer coefficient k_{mix} is independent of current density in the laboratory cell. For CE as a function of cathodic current density (Fig. 3) there is a deviation of model prediction from experimental values at low current densities. This is likely to be due to decreasing rate of anode gas evolution with decreasing current density, and thus decreased bubble induced convection in the electrolyte. Figure 10 shows a better fit of the model curve to experimental values, compared to Fig. 3, obtained by including a linear increase of k_{mix} (k'_{mix}) with increasing current density:

$$k'_{mix} = (0.75 + 0.294\ i_c)k_{mix} \qquad (14)$$

It must be emphasized that Equation 14 is specific only for the present laboratory cell with uniform cathode current density, and should not be used for calculations in industrial cells. For calculations of the influence of cell geometry and current distribution on local and overall cell current efficiency in industrial

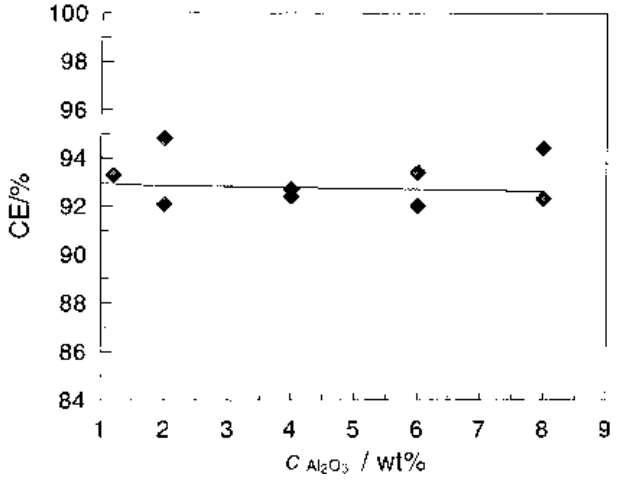

Fig. 8. Current efficiency, CE, as a function of electrolyte alumina concentration, $c_{Al_2O_3}$. Cathodic current density 0.85 A cm^{-2}, temperature 980 °C, NaF/AlF_3 molar ratio 2.5 and 5 wt% CaF_2. Experimental values (points) and CE model curve.

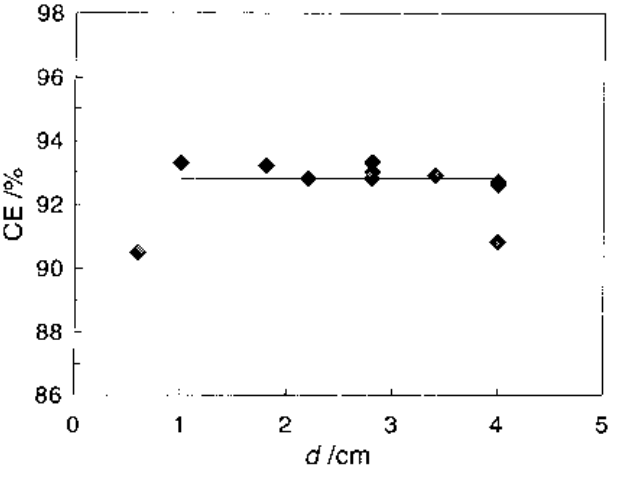

Fig. 9. Current efficiency, CE, as a function of interpolar distance, *d*. Cathodic current density 0.85 A cm^{-2}, temperature 980 °C, NaF/AlF_3 molar ratio 2.5, 4 wt% Al_2O_3 and 5 wt% CaF_2. Points: experimental values, solid line: CE model.

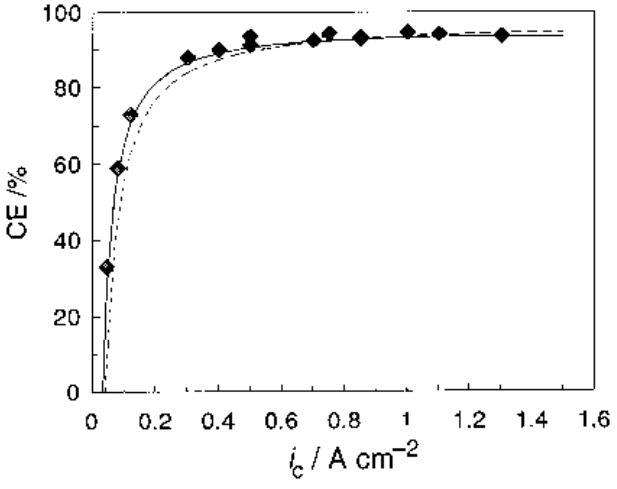

Fig. 10. Current efficiency, CE, as a function of cathodic current density, i_c. Temperature 980 °C, NaF/AlF_3 molar ratio 2.5, 5 wt% CaF_2 and 4 wt% Al_2O_3. Points: experimental values, full drawn curve: CE model with correction for variation of k_{mix} with i_c (Equation 14), and dotted curve: CE model with constant k_{mix}.

cells, it is necessary to know how the mass transfer conditions vary across the cell, for example, by calculation of anode gas bubble induced and magnetic field induced electrolyte flow. Knowledge of current distribution and local variations of the mass transfer coefficient k_{mix} in industrial cells, gives the necessary basis to calculate overall current efficiency by working out the integral,

$$I_{loss} = \int_0^A i_{loss} dA \qquad (15)$$

The sum $I_{Al} + I_{loss}$ represents the total cell current if there are no short circuits. Such calculations may be of value in the design of industrial cells. By combination of the present CE model with calculations of frozen side ledge geometry, cell thermal balance, current distribution, magnetic fields and fluid dynamic flow (heat transfer coefficients), valuable information about the optimum cell design with respect to current efficiency can be attained. To achieve high current efficiency values in industrial cells, it is advantageous to have a stable and adequately thick frozen side ledge and to have a metal pool which does not extend far outside the vertical projection of the anodes.

Figure 7 shows that there is a deviation between model prediction of CE and experimental values at low concentrations of CaF_2 in the electrolyte. This may possibly be due to altered mass transfer or surface phenomena upon addition of CaF_2. It is known that surface-active agents may slow down chemical reactions by squeezing out less surface-active reactants from the interface [27]. In the $NaF–AlF_3–Al$ system, Dewing and Desclaux [28] found a considerable increase of interfacial tension with decreasing NaF/AlF_3 ratio, and explained this by metallic sodium being a surface active substance adsorbed to the interface. It is possible that calcium may participate in surface adsorbtion processes on the aluminium–electrolyte interface, and thereby affect the adsorbtion of sodium. The deviation between model predictions of CE and experimental values at 0% CaF_2 (Fig. 7) can be explained by a possible 20% decrease of k_{mix} upon addition of CaF_2 to the electrolyte.

3.10. *Uncertainty in determined CE*

An estimation of the uncertainty in determined CE was carried out, by calculation of the standard deviations from the respective average values, for all parallel runs in the present study. The parallel runs at temperatures higher than 1000 °C gave the highest standard deviations. All parallels included, the average absolute standard deviation was 0.5% CE, while exclusion of temperatures higher than 1000 °C gave an average standard deviation of 0.3% CE. For normal industrial temperatures the uncertainty of determined CE in the present laboratory cell is estimated to ±0.6%, calculated at ±2 standard deviations.

The use of a stainless steel plate as cathode substrate inevitably leads to iron dissolution into the molten aluminium phase. Analysis of the metal pool after electrolysis revealed an iron concentration of 6–8 wt%, roughly in agreement with equilibrium values [29]. The alloy composition corresponds to an activity of aluminium of approximately 0.93, a deviation from unit activity which, by employment of the present CE model, is calculated to give less than 0.2% error in determined CE [5].

4. Conclusion

The results of the present experimental study of current efficiency show a non-linear decrease of CE with increasing electrolyte temperature, a close to linear decrease of CE with increasing NaF/AlF_3 ratio in the electrolyte, nonlinear increase of CE with increasing cathodic current density, a slight increase of CE with increasing electrolyte CaF_2 concentration, and no influence of electrolyte Al_2O_3 concentration on CE. The results are believed to be generally representative for isolated primary dependencies in industrial cells. This is due to the laboratory cell design, with reproducible convective conditions, and a flat cathode surface which gives uniform cathode current distribution. The results are satisfactory described by the present current efficiency model, and supports the basic theory on which the model is based.

Acknowledgements

Financial support from The Research Council of Norway and from Norwegian aluminium industry is gratefully acknowledged. The work was performed in cooperation with the Electrolysis Group, SINTEF Materials Technology.

References

[1] H. Ginsberg and H. C. Wrigge, *Metall.* **26** (1972) 997.
[2] Å. Sterten and P. A. Solli, *J. Appl. Electrochem.* **25** (1995) 809.

[3] *Idem, ibid.* **26** (1996) 187.
[4] P. A. Solli, T. Eggen, E. Skybakmoen and Å. Sterten, *ibid.* **26** (1996) 1019.
[5] P. A. Solli, 'Current Efficiency in Aluminium Electrolysis Cells', Thesis, Norwegian Institute of Technology, University of Trondheim, Norway (1993).
[6] Å. Sterten, *J. Appl. Electrochem.* **18** (1988) 473.
[7] Å. Sterten and I. Mæland, *Acta Chem. Scand.* **A39** (1985) 241.
[8] R. Ødegård, 'Solubility and Electrochemical Behaviour of Al and Al_4C_3 in Cryolitic Melts', Thesis, Norwegian Institute of Technology, University of Trondheim, Norway (1986).
[9] J. Thonstad and S. Rolseth, *Electrochim. Acta* **23** (1978) 221.
[10] *Idem, ibid.* **23** (1978) 233.
[11] S. Gjerstad and N. E. Richards, *J. Electrochem. Soc.* **113** (1966) 68.
[12] P. Barat, T. Brault and J. P. Saget, 'Light Metals', vol. 1 (edited by H. Forberg), Proceedings of the 104th TMS annual meeting (1975), p. 37.
[13] R. A. Lewis, *J. Metals* **19** (1967) 30.
[14] J. W. Burck and D. Fern, 'Light Metals' (edited by T. G. Edgeworth), Proceedings of the 100th TMS annual meeting (1971), p. 123.
[15] B. Berge, K. Grjotheim, C. Krohn, R. Næumann and K. Tørklep, 'Light Metals' (edited by S. R. Leavitt), Proceedings of the 105th TMS annual meeting (1976), p. 23.
[16] E. W. Dewing, *Metall. Trans. B* **22** (1991) 177.
[17] J. Thonstad, *Can. J. Chem.* **43** (1965) 3429.
[18] R. T. Poole and C. Etheridge, 'Light Metals' (edited by K. B. Higbie), Proceedings of the 106th TMS annual meeting (1977), p. 163.
[19] T. R. Alcorn, C. J. McMinn and A. Tabereaux, 'Light Metals' (edited by L. G. Boxall), Proceedings of the 117th TMS annual meeting (1988), p. 683.
[20] C. Szeker, *Acta Technica Acad. Sci. Hung.* **10** (1954) 19.
[21] P. Fellner, K. Grjotheim, K. Matiasovsky and J. Thonstad, *Can. Met. Quart.* **8** (1969) 245.
[22] K. Grjotheim, M. Malinovsky, K. Matiasovsky, A. Silny and J. Thonstad, *ibid.* **11** (1972) 295.
[23] B. Lillebuen, S. A. Ytterdahl, R. Huglen and K. A. Paulsen, *Electrochim. Acta* **25** (1980) 131.
[24] K. A. Paulsen, J. Thonstad, S. Rolseth and T. Ringstad, 'Light Metals' (edited by S. K. Das), Proceedings of the 122nd TMS annual meeting (1993), p. 233.
[25] M. J. Leroy, T. Pelekis and J. M. Jolas, 'Light Metals' (edited by R. D. Zabreznik), Proceedings of the 116th TMS annual meeting (1987), p. 291.
[26] S. Rolseth, A. Solheim and J. Thonstad, Proceedings of the International Symposium on Reduction and Casting of Aluminium vol. 6, (edited by C. Bickert) Metallurgical Society of the Canadian Institute of Mining and Metallurgy, Pergamon Press, Montreal (1988), p. 229.
[27] F. D. Richardsson, 'Physical Chemistry of Melts in Metallurgy', vol. 2, Academic Press, London (1974), p. 480.
[28] E. W. Dewing and P. Desclaux, *Met. Trans. B.* **8** (1977) 555.
[29] T. B. Massalski, J. L. Murray, L. H. Bennett and H. Baker, 'Binary Alloy Phase Diagrams', vol. 1, Am. Soc. Met., OH (1986), p. 112.